TISSUE ENGINEERING: Part C
Volume 25, Number 9, 2019

DOI: 10.1089/ten.tec.2019.0151

termis
Tissue Engineering
& Regenerative Medicine
International Society

METHODS ARTICLE

LED-Based Photoacoustic Imaging for Monitoring Angiogenesis in Fibrin Scaffolds

Yunhao Zhu, MS,[1,2] Xiaofang Lu, MD,[3] Xiaoxiao Dong, MS,[3,4] Jie Yuan, PhD,[2] Mario L. Fabiilli, PhD,[1,3,5] and Xueding Wang, PhD[1,3]

Vascularization of engineered constructs is required to integrate an implant within the host blood supply. The ability to noninvasively monitor neovascularization of an implanted construct is ultimately critical for translation. Laser speckle contrast analysis (LASCA), a widely used imaging technique within regenerative medicine, has high spatial resolution but offers limited imaging depth and is only sensitive to perfused blood vessels. As an emerging technology, photoacoustic (PA) imaging can provide centimeters of imaging depth and excellent sensitivity in vascular mapping. PA imaging in combination with conventional ultrasound (US) imaging offers a potential solution to this challenge in regenerative medicine. In this study, we used an LED-based PA-US dual system to image and monitor angiogenesis for 7 days in fibrin-based scaffolds subcutaneously implanted in mice. Scaffolds, with or without basic fibroblast growth factor (bFGF), were imaged on day 0 (i.e., postimplantation), 1, 3, and 7 with both LASCA and PA-US imaging systems. Quantified perfusion measured by LASCA and PA imaging were compared with histologically determined blood vessel density on day 7. Vessel density corroborated with changes in perfusion measured by both LASCA and PA. Unlike LASCA, PA imaging enabled delineation of differences in neovascularization in the upper and the lower regions of the scaffold. Overall, this study has demonstrated that PA imaging could be a noninvasive and highly sensitive method for monitoring vascularization at depth in regenerative applications.

Keywords: photoacoustic imaging, optical imaging, angiogenesis, fibrin

Impact Statement

Noninvasive imaging techniques provide insight into physiology that is complementary to tissue morphology obtained by invasive histology. Optical imaging techniques, such as laser speckle contrast analysis, are used *in vivo* to longitudinally evaluate vascularization. Despite their high spatial resolution, these techniques have a limited imaging depth. In this study, we demonstrate how a dual LED-based photoacoustic (PA) and ultrasound system can delineate changes in perfusion at depth within scaffolds containing basic fibroblast growth factor. Perfusion changes detected by PA corroborated with vessel density. PA imaging could be a noninvasive and sensitive method for evaluating vascularization at depth in larger constructs.

Introduction

Tissue engineering utilizes cells, biomaterials, and signaling molecules to create biological constructs that facilitate the regeneration of impaired or injured tissue and organs. Hydrogels are widely used in tissue engineering as biocompatible matrices for the encapsulation and delivery of cells and regenerative factors. Fibrin is commonly used in tissue engineering as a foundational matrix for construct fabrication.[1–4] Except for thin or avascular tissues, engineered constructs require proper vasculature to facilitate transport of oxygen, nutrients, and waste, thus maintaining construct viability. The spontaneous ingrowth of blood vessels into scaffolds can be slow[5,6] and cells, especially at the center of

[1]Department of Biomedical Engineering, University of Michigan, Ann Arbor, Michigan.
[2]Department of Electronic Science and Engineering, Nanjing University, Nanjing, China.
[3]Department of Radiology, University of Michigan, Ann Arbor, Michigan.
[4]Department of Ultrasound, The Second Affiliated Hospital of Army Medical University, Chongqing, China.
[5]Department of Applied Physics Program, University of Michigan, Ann Arbor, Michigan.

implants, can become hypoxic, thus reducing construct viability. Strategies to stimulate vessel growth include the development of prevascularized implants and the delivery of exogenous proangiogenic growth factors (GFs).[7–10]

The ability to noninvasively monitor neovascularization of an implanted scaffold is critical for translation of engineered constructs. Monitoring would be especially beneficial for scaffolds that can be modulated using external stimuli. For example, scaffolds have been developed that respond to magnetism,[11] light,[12] and electricity.[13] Recently, we developed a composite hydrogel, termed an acoustically responsive scaffold (ARS), where release of encapsulated payloads was modulated in a spatiotemporally controlled manner using focused pulsed ultrasound (US).[4,14] The delivery of basic fibroblast growth factor (bFGF) from ARSs was modulated noninvasively using US, which resulted in significant increases in perfusion and neovascularization in an *in vivo* study.[15] Therefore, for scaffolds that can be actively modulated, noninvasive monitoring could provide a means for the planning, guidance, and monitoring of treatment (e.g., delivery of proangiogenic GFs). This would enable personalization of the therapy based on the actual response of the construct after implantation.

Laser speckle contrast analysis (LASCA), which we used in our previous study, and laser Doppler perfusion imaging (LDPI) techniques are widely employed in regenerative studies with mouse, rat, and rabbit models because of the good sensitivity of each method to neovascularization. However, the imaging depths of both LASCA and LDPI techniques are limited ($\sim$1 mm).[16–18] Other commonly used optical methods, such as optical resolution photoacoustic microscopy and optical coherence tomography, also have relatively low imaging depths ($\sim$0.5–1.5 mm) in tissue.[19–21] Techniques such as magnetic resonance imaging, microcomputed tomography, positron emission tomography, single-photon emission computed tomography, and contrast-enhanced US imaging methods are able to map blood perfusion at depth, but often require the injection of contrast agents, radiotracers, or the use of ionizing radiation.[22–25] In addition, Doppler US can be insensitive to small diameter blood vessels with low flow velocities, which typically appear in early stages of angiogenesis.[19,25–27]

The emerging photoacoustic (PA) imaging technique in combination with established US imaging could solve this challenge in regenerative medicine. PA imaging can provide centimeters of imaging depth, is nonionizing, and is highly sensitive in detecting blood despite its flow speed. The B-mode US modality in the combined imaging system can provide high-resolution structural information in parallel.[28–31] PA imaging has been previously explored for monitoring neovascularization in scaffolds, and has shown exciting results.[32,33] These studies were based on class IV lasers as the light sources that have associated safety concerns, high equipment costs, and are relatively immobile. These concerns could be addressed by PA imaging using an LED light source.[34,35] In this article, we used an LED-based PA-US dual system to image and monitor angiogenesis in subcutaneously implanted fibrin-based scaffolds with a 7-day longitudinal study. Subcutaneous implantation of scaffolds is commonly used in tissue regeneration studies, and a model we have used before.[15,36] In this study, we focus on analyzing the performance of LASCA and LED-based PA-US imaging systems and compare the results with vessel density obtained through immunohistochemical staining.

Methods

In situ *polymerization of fibrin scaffolds*

This *in vivo* research was conducted with the approval of the Institutional Animal Care and Use Committee at the University of Michigan. Female BALB/c mice ($n=5$, 19.2 ± 1.0 g, 4–6 weeks old; Charles River Laboratories, Wilmington, MA) were anesthetized with isoflurane (5% for induction and 1.5% for maintenance). The lower dorsal hair was removed by shaving and applying depilatory cream (Nair, Church & Dwight Co, Ewing, NJ). The skin was disinfected with povidone-iodine (Betadine, Purdue Products L.P., Stamford, CT). The scaffold mixture (0.3 mL per implant) was injected subcutaneously using a 20-gauge needle (Becton Dickinson, Franklin Lakes, NJ) at two locations within the lower dorsal region and allowed to polymerize for 2 min before removal of the needle. The scaffold mixture consisted of the following: 10 mg/mL bovine fibrinogen (Sigma-Aldrich, St. Louis, MO) in Dulbecco's modified Eagle's medium (Life Technologies, Grand Island, NY), 0.05 U/mL bovine aprotinin (Sigma-Aldrich), 125 μg/mL Alexa Fluor 647-labeled human fibrinogen (Molecular Probes, Eugene, OR), 2 U/mL bovine thrombin (Thrombin-JMI, King Pharmaceuticals, Bristol, TN), 34 μg/mL bovine serum albumin (Sigma-Aldrich), and 6.6 mU/mL porcine heparin (EMD Millipore, Burlington, MA). Each mouse received one implant with 1 μg of bFGF (EMD Millipore) per scaffold, whereas the contralateral implant served as a negative control (i.e., 0 μg bFGF). The placement of the negative control (i.e., left or right side) was randomized in all mice.

LASCA and LED-based PA imaging of scaffolds

The detailed experimental schedule, including scaffold implantation and imaging, is shown in Figure 1. On days 2, 4, and 6, 50 μL of 20 μg/mL bFGF was subcutaneously injected into scaffolds initially containing bFGF on day 0 (i.e., +bFGF). Phosphate buffered saline (Life Technologies) was injected into the negative control scaffolds (i.e., −bFGF). LASCA and PA imaging procedures were done in no particular order on days 0, 1, 3, and 7. A brief schematic diagram of LASCA/PA imaging is also shown in Figure 1. After the completion of imaging on day 7, the mice were euthanized and the implants were retrieved for histology.

LASCA imaging. The mice were anesthetized with isoflurane and imaged with a PeriCam PSI HR (Perimed, Ardmore, PA) LASCA system to quantify the relative perfusion within the implant regions. The mice were imaged on days 0 (i.e., immediately after implantation), 1 (i.e., the first day), 3, and 7. All images were acquired with a 10 cm distance between the scanner and implant, resulting in a resolution of 20 μm/pixel. Pimsoft software (Perimed) was used for image acquisition and processing. A total of 30 images per implant per time point were acquired at a rate of 0.096 images per second with a field of view of 2.0×2.8 cm. A near-infrared laser (785 nm) was used as the light source. Every six images were averaged to create a total of five averaged images per implant per time point. The average relative perfusion was computed within elliptical regions of interest (ROIs; major axis: 1.1 cm, minor axis: 1 cm) encompassing each implant. The percentage change in perfusion was calculated for each implant relative to the average perfusion on day 0.

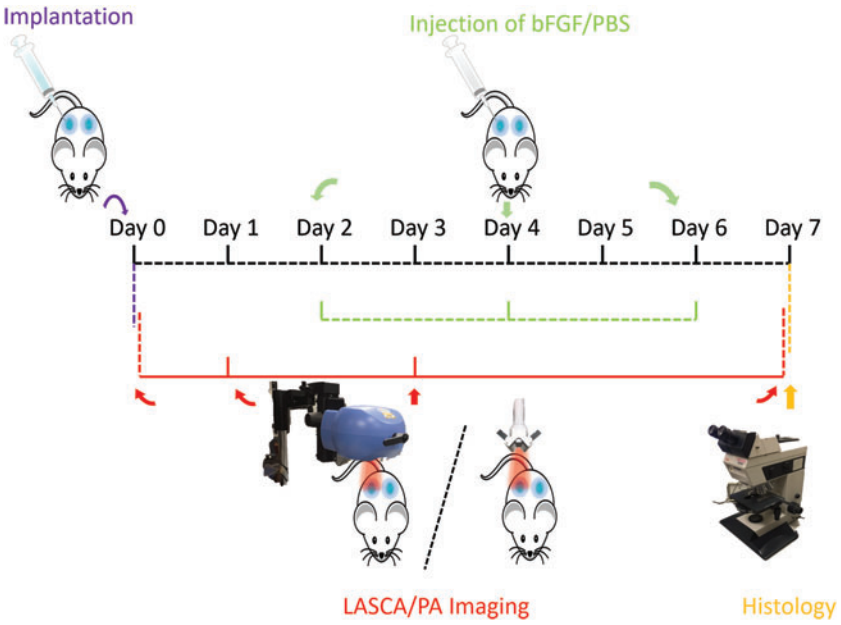

FIG. 1. The 7-day longitudinal experimental schedule. Scaffold implantation was done on day 0. LASCA/PA imaging was on day 0 (i.e., after implantation), 1, 3, and 7. bFGF or PBS was injected subcutaneously adjacent to each scaffold every 2 days. Scaffolds were retrieved on day 7 for H&E and CD31 staining. Each mouse received two scaffolds represented by the *blue areas*. bFGF, basic fibroblast growth factor; H&E, hematoxylin and eosin; LASCA, laser speckle contrast analysis; PA, photoacoustic; PBS, phosphate buffered saline. Color images are available online.

LED-based PA-US imaging. Mice were anesthetized with isoflurane and secured to a platform in a prone position. The platform was partially submerged in a 37°C water tank such that the implanted scaffolds were completely submerged for imaging. The LED-based PA imaging system (AcousticX, Cyberdyne, Inc., Tsukuba, Japan) has been introduced before and was employed in this study.[34] Two LED bars (850 nm wavelength, dimensions: 50 × 7 mm), which were positioned on either side of a linear 7 MHz US probe, had an illumination projection angle of 45° with respect to the US imaging plane. The LED output energy was 400 μJ/pulse. Since the PA and US images were acquired by the same US transducer array, the two modalities were inherently co-registered. The imaging probe was fixed to a translational stage (OSMS20-85, OptoSigma, Tokyo, Japan) with a resolution of 2 μm/pulse for data acquisition. A series of two-dimensional (2D) US and PA images of each scaffold were acquired at 10 Hz in the sagittal orientation while the probe was translated at 0.5 mm/s across the volume of the implant. Scanning took ~20 s for each implant.

Each series of 2D PA images were postprocessed for analysis. ROIs, encompassing the implanted scaffolds, were selected based on the B-mode US images. The US images also enabled us to determine the central plane of the scaffold. A series of PA frames within 2.5 mm (i.e., from –2.5 to 2.5 mm) of the central plane was then projected onto the central frame, which yielded a maximum intensity projected (MIP) PA image for display. For quantification, the PA signal within the implant region was calculated as the summation of pixel intensity in the ROI divided by the ROI area in each frame (i.e., averaged PA intensity). For additional analysis, each scaffold was separated into upper and lower layers. The upper layer was delineated by an ROI encompassing the uppermost ~3 mm thickness (approximate to mean free path of light at 785 nm in skin) of the scaffold (i.e., beneath the skin surface).[37] The lower layer was defined as the ROI encompassing the rest of scaffold (i.e., entire scaffold minus the upper layer). The percentage change in PA intensity was calculated for each implant relative to the averaged PA intensity on day 0.

Histology

Retrieved implants were fixed overnight in aqueous buffered zinc formalin (Formalde-Fresh; Fisher Scientific, Waltham, MA). Implants were then transferred to 70% ethanol until they were processed and embedded in paraffin. The paraffin-embedded tissues were cut into 5 μm thick serial sections and placed on precleaned glass slides (Fisherbrand Superfrost Plus; Thermo Fisher Scientific, Waltham, MA) for histological analysis. Tissue sections were stained with Modified Harris Formulation hematoxylin (Ricca Chemical Company, Arlington, TX) and aqueous eosin Y solution (0.25% [w/v] in 57% [v/v] alcohol; Sigma-Aldrich) (H&E) to visualize the overall tissue morphology. Immunostaining of blood vessels was performed using a rabbit anti-mouse CD31 primary antibody (ab124432; Abcam, Cambridge, MA) combined with a goat anti-rabbit secondary labeled polymer-horseradish peroxidase conjugate (Envision+ System-HRP (DAB); Dako North America, Inc., Carpinteria, CA), as described previously.[15,36] Negative controls with a rabbit IgG polyclonal isotype control (ab37415; Abcam) as the primary antibody confirmed the specificity of the CD31 staining. Tissue sections were visualized and photographed with a Leica DMRB light microscope (Leica Microsystems, Buffalo Grove, IL). Granulation layers between the skin and the scaffold (upper layer) as well as between the scaffold and underlying muscle (lower layer) from each tissue section—with five images per tissue layer—were analyzed manually for blood vessel formation per unit area. Blood vessel counting was done, in a blinded manner, by three separate individuals. Blood vessels were identified in CD31-stained tissues at 20× magnification by defined lumens and complete enclosure of the lumen.

Statistics

All statistical analyses were performed using GraphPad Prism software (GraphPad Software, Inc., La Jolla, CA). All data are expressed as the mean ± standard error of the mean of measured quantities. Statistically significant differences

of all other data sets were determined with a Student's *t*-test corrected for multiple comparisons using the Holm–Sidak method, with differences deemed significant for $p < 0.05$.

Results

LASCA imaging

LASCA imaging was employed to monitor the perfusion noninvasively and longitudinally in and around the subcutaneous implants placed in the lower dorsal region. Figure 2A displays a macroscopic image of a mouse with implants along with longitudinal perfusion images from days 0 to 7. The ROIs are marked by black and red ellipses, indicating the −bFGF and +bFGF implants, respectively. The LASCA images qualitatively show more perfusion in the +bFGF scaffolds than the −bFGF scaffolds in the days after implantation.

Figure 2B shows a quantitative analysis of the ROIs, which was based on computing a relative change in average perfusion units for a given implant relative to day 0. Overall perfusion tended to increase over time, with the greatest increases observed for the +bFGF group relative to the −bFGF group, which approached statistical significance on day 7 ($p = 0.055$).

LED-based PA imaging

We acquired 2D images of the implanted scaffolds and postprocessed three-dimensional (3D) videos with the LED-based PA-US imaging system. Figure 3A shows a series of 2D US-PA images from a +bFGF scaffold on day 7 at different scan positions (i.e., sagittal planes). The PA signal, in red, is overlaid on the B-mode US image, in grayscale. Figure 3B shows a series of longitudinal MIP US-PA images of both scaffolds from the same mouse. Qualitatively, the +bFGF implant has a PA intensity that increased over time, especially adjacent to the skin. Some signal appears within the scaffold, likely due to the projection of multiple images into a single plane. With the −bFGF implant, only point-like contrast was detected in the scaffold, with no obvious trend during the 7-day experiment. The PA signal from the +bFGF and −bFGF scaffolds appeared similar on day 0. The results on different days of each mouse are normalized with day 0 and then compared the percentage change. The greatest difference was observed on day 7, which was also consistent with the LASCA results. On day 7, the +bFGF scaffold displayed a strong PA signal, especially between the skin and upper layer of the implant. Some PA signal was observed in the −bFGF scaffold, although at a lower level compared with the +bFGF scaffold.

The height and length of the implanted scaffolds measured using B-mode US, are shown in Figure 4A, B. The height and length of scaffolds showed a decreasing trend with days. The PA data were quantified by calculating the normalized intensity, relative to day 0 for each scaffold, as shown in Figure 4C–E. Figure 4C shows the change in PA

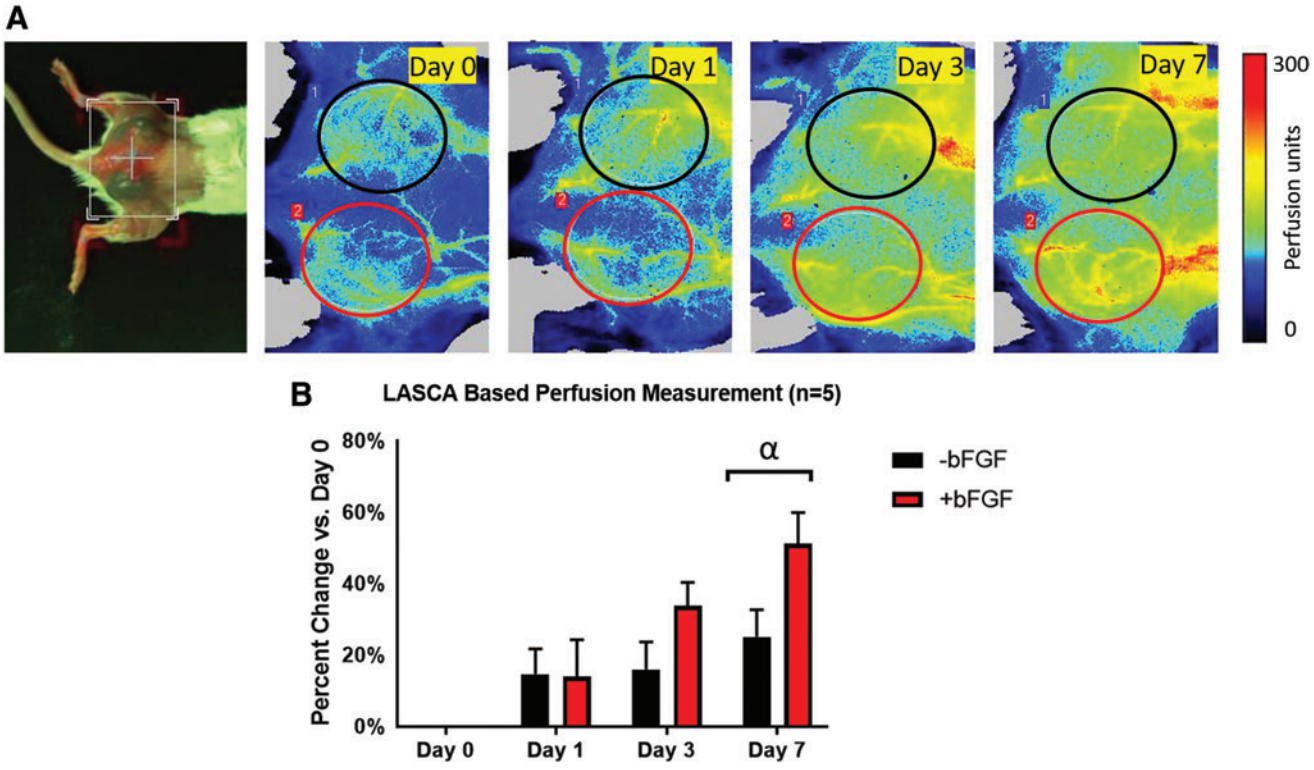

FIG. 2. **(A)** Photo of dorsal view (*leftmost*) and longitudinal LASCA images of a mouse with two subcutaneous implants. The ROIs were chosen based on the physical location of the implants, and are denoted by colored ellipses (*red* for +bFGF and *black* for −bFGF). For all LASCA images, the caudal direction is toward the *left*. ROI dimensions: 1.1 cm (major axis), 1.0 cm (minor axis). **(B)** Quantification of the change in perfusion relative to day 0, based on an ROI analysis of the LASCA images, shows an overall increase in perfusion over time. The greatest change in perfusion was observed on day 7, with +bFGF scaffolds trending toward greater perfusion than −bFGF scaffolds. α: −bFGF versus +bFGF on day 7 ($p = 0.055$). ROIs, regions of interest. Color images are available online.

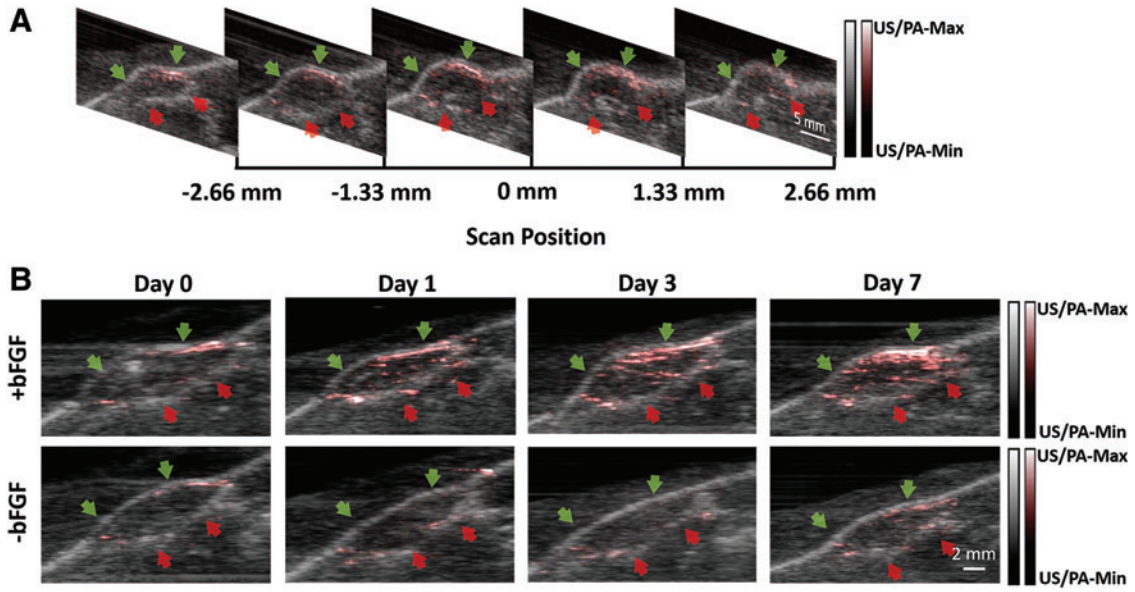

FIG. 3. Longitudinal LED-based PA-US imaging of two subcutaneous implants. *Green* and *red arrows* indicate the *upper* and *lower* edges of the scaffold, as determined through the B-mode US. **(A)** A series of two-dimensional US-PA images from a +bFGF scaffold on day 7 at different scan positions. Note that only images within the range of −2.5 to 2.5 mm are used for MIP image. **(B)** A series of longitudinal MIP US-PA images of +bFGF and −bFGF scaffolds from the same mouse. PA intensity represented in *red* has the greatest difference on day 7. MIP, maximum intensity projected; US, ultrasound. Color images are available online.

signal for +bFGF and −bFGF scaffolds (i.e., the entire scaffold) over the course of the experiment. Figure 4D, E showed the change in PA for the upper and lower layers, respectively. 3D renderings of the PA signal within the scaffold volume on days 1, 3, and 7 can be found in the Supplementary Videos S1–S3.

Morphology and vascularization of scaffolds

Representative H&E and CD31 stained images of +bFGF and −bFGF implants are shown in Figure 5. Figure 5A and B show the H&E staining of a scaffold with adjacent deep muscle tissue. Figure 5C and D show the CD31 staining of the same regions in Figure 5A, B. Figure 5E and F are the CD31 staining of vessels from the upper layer and Figure 5G, H are from lower layer. The dark region indicates the blood vessels stained in the scaffolds. Figure 5A, C, E, and G are from +bFGF and Figure 5B, D, F, and H are from −bFGF. Qualitatively, there are more stained vessels in the +bFGF scaffold versus the −bFGF scaffold.

Figure 6 shows the overall blood vessel density, obtained through CD31 staining, which is a commonly used metric. All the +bFGF group exhibited significantly greater ($p < 0.001$) vessels than the −bFGF group. Figure 6A–C are the vessel counts per area of the entire scaffold, the upper layer, and the lower layer, respectively. The general trends of vasculature marked by CD31 on day 7 are well matched with Figure 4C–E, with the upper layer showing the highest vessel density and PA signal.

Discussion

PA imaging could noninvasively provide high optical contrast, label-free images of vasculature, and microvasculature with desired resolution and penetration depth for assessing implanted tissue constructs. A conventional class IV laser can provide powerful energy for PA imaging. However, safety concerns, high equipment cost, and immobility may impede laser-based PA imaging in having a small footprint and becoming a point-of-care technique. These limitations are not present with PA imaging using a LED light source. The American National Standards Institute (ANSI) has detailed safety limits for laser exposure to the skin and the eye. Within the ANSI safety limits, PA is safe for clinical applications. However, replacing conventional class-IV lasers with LED light sources could further improve safety and accelerate the clinical acceptance of emerging PA imaging technology. In addition, compared with expensive class-IV laser systems, an LED-based light source is much lower in both owning and operating costs. With an imaging depth up to 2 cm and resolution around 200 μm, the LED-based PA-US imaging system has been explored for many applications in biomedical fields but has not been used in tissue engineering, to our knowledge. As discussed previously, potential clinical applications of LED-based PA imaging include the assessment of peripheral microvascular function, diagnosis of inflammatory arthritis, and detection of head and neck cancer.[34] In this study, we focus on mapping microvasculature and its potential application in regenerative medicine, specifically monitoring angiogenesis in fibrin scaffolds.

The use of noninvasive imaging for monitoring neovascularization is ultimately crucial for the translation of tissue engineering-based technologies. LASCA, which has been used in tissue regeneration studies, is inherently limited in terms of imaging depth, although the spatial resolution is high. In this study, host cells invaded the implanted scaffold at the periphery, ultimately leading to neovessel formation, as seen

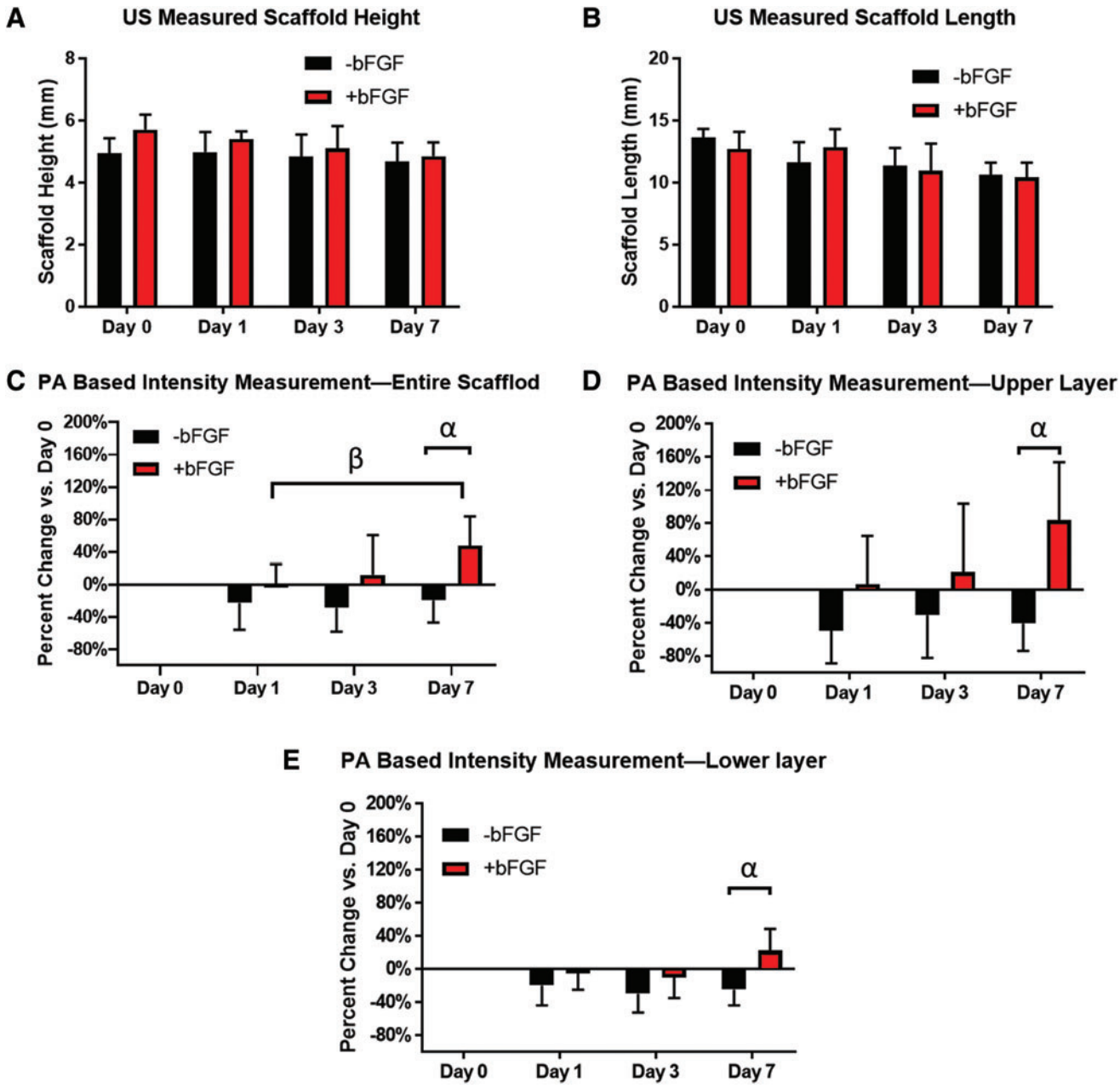

FIG. 4. Quantification of scaffold size and blood flow, based on US images and PA signals, respectively. **(A, B)** The height and length of the scaffold changing with days resolved by US images. **(C–E)** The normalized PA intensity of the entire scaffold, *upper layer*, and the *lower layer* based on the baseline of day 0, respectively. Statistically significant differences ($p < 0.05$) are denoted as follows: α, −bFGF versus +bFGF on day 7 based on PA measurement; β, +bFGF on day 1 versus +bFGF on day 7 based on PA measurement. Color images are available online.

through immunohistochemical staining. Vessel formation was observed in both the upper and lower layers of the scaffold, the latter of which would not be detected using LASCA. Optical methods such as LASCA are limited due to the scattering of light, which can become significant after penetrating ~ 1 mm in biological tissue.

There was a decrease in PA signal when comparing day 0 versus day 1, which was sustained for the −bFGF group for the duration of the 7-day study. One possible reason is that injection of the scaffold during implantation caused some minor bleeding in the subcutaneous space. This blood, which was later resorbed by the tissue, enhanced the PA signal on day 0. As this extravascular blood was not flowing, it did affect the results from LASCA.

In our previous study, we utilized LASCA to monitor perfusion within subcutaneous fibrin implants in mice for the course of 14 days.[15] There was no significant difference, detected by LASCA, when comparing fibrin only scaffolds with fibrin scaffolds containing 1 μg bFGF. Yet, based on C31 staining, there was a significant difference in vessel density between the two groups. However, a key difference exists between these two studies. In this study, bFGF was

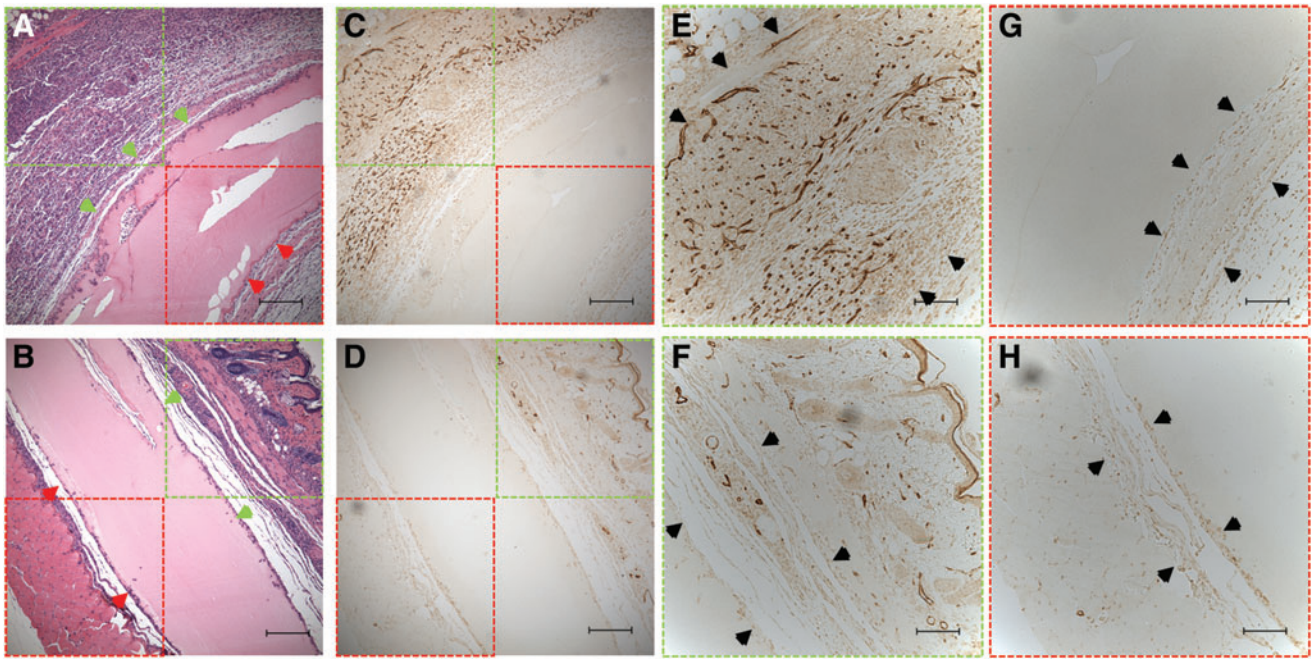

FIG. 5. H&E images of implanted +bFGF **(A)** and −bFGF **(B)** scaffolds. *Green arrows* indicate the interface between the scaffold and *upper layer* tissue. *Red arrows* indicate the interface between the scaffold and lower layer tissue. **(C, D)** The CD31 staining of the same scaffold of **(A, B)**. **(E, F)** The CD31 staining of vessels from the *upper layer*. **(G, H)** The same from *lower layer*. The dark region indicates the blood vessels stained in the scaffolds. The *black arrows* in **(E–H)** mark the adjacent tissue. **(A, C, E, G)** are from +bFGF and **(B, D, F, H)** are from −bFGF. Scale bar: **(A–D)** 200 μm, **(E–H)** 100 μm. Color images are available online.

loaded into the scaffold upon implantation and then injected every 2 days. In the previous study, bFGF was only incorporated into the scaffold upon implantation. Although bFGF exhibits strong binding to fibrin, a burst release of bFGF occurs within 1–2 days when the growth factor was directly incorporated into fibrin scaffolds.[38,39] After this initial burst release, minimal additional release of bFGF occurs. Therefore, it is likely that, by readministering bFGF, as was done in this study, the level of the growth factor was maintained at a sufficiently elevated level in the implant region to lead to greater changes in perfusion.

The LASCA and PA results on day 7 were consistent with blood vessel density measured through CD31 staining. The densities of vessels in the lower and upper layers were similar for the −bFGF group. For the +bFGF group, there was a significantly higher vessel density in the upper layer compared with the lower layer. Since bFGF was injected subcutaneously in the skin overlying the implanted scaffold, this finding may be attributed to the injection location, which would have generated a higher concentration of bFGF adjacent to the upper layer. The blood vessel density and PA signal in the upper and lower regions can also be compared. Based on the results shown in Figures 4 and 6, we found the angiogenesis ratio (i.e., +bFGF/−bFGF based on histology/PA results) on day 7 is 5.1 based on histology in whole scaffolds, whereas PA-based result shows the ratio is 1.83 (PA absolute intensity used

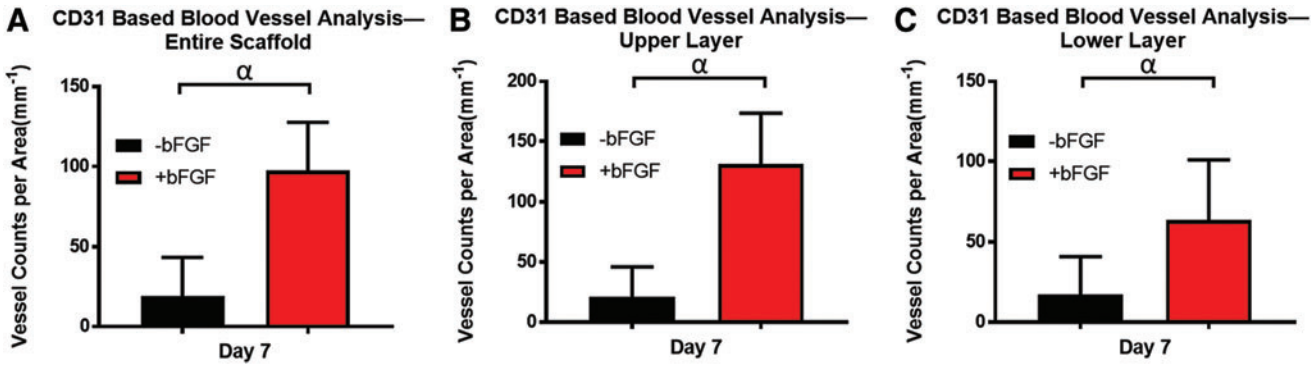

FIG. 6. **(A–C)** The vessel counts per area of the entire scaffold, the *upper layer*, and the *lower layer*, respectively. Statistically significant differences ($p < 0.001$) are denoted as follows: α, −bFGF versus +bFGF based on CD31 measurement. Color images are available online.

for day 7 = 100% + percentage change on day 7, then the ratio was calculated by +bFGF/−bFGF). Histology versus PA ratios of +bFGF/−bFGF at the upper layer is 6.3 versus 3.9 and the lower layer is 3.05 versus 1.36, which also means the upper layer is dominated (about twofold of lower layer). This also demonstrated that LED-based PA-US imaging can resolve and quantify the vasculature in the different layers in the scaffolds. We performed the *t*-test with the null hypothesis and found the significant difference ($p < 0.05$) in the upper layer, lower layer, or both, between the +bFGF and −bFGF groups.

PA imaging also has the potential to provide functional images in which physiological parameters such as blood oxygen saturation, pH value, and flow velocity can be measured.[31,40,41] Therefore, this technique has the potential to be used not only to monitor neovascularization in the scaffolds but also to provide crucial functional information to guide the therapy in preclinical and clinical settings. The LED-based PA imaging system also has the advantages of low price, good safety, and high mobility when compared with those equipped by conventional class IV lasers. Thus, LED-based PA imaging could be a useful tool within tissue engineering and regenerative medicine for noninvasive and longitudinal assessment of vascularization.

In this study, we longitudinally monitored neovascularization in mice containing subcutaneous fibrin implants with both LASCA and an LED-based PA imaging. bFGF was used to induce angiogenesis in the implant regions. The perfusion in the implants measured by the imaging techniques were validated by quantitative histology. PA imaging was able to cover the entire scaffold volume, and enabled delineation of neovascularization in the upper and the lower regions of the scaffold, respectively. PA imaging results matched well with the findings from histology, suggesting that PA imaging could be a noninvasive and highly sensitive method for monitoring angiogenesis at depth in regenerative applications.

Disclosure Statement

No competing financial interests exist.

Funding Information

This study was supported by NIH Grant R01HL139656 (M.L.F.) and R01AR060350 (X.W.).

References

1. Shaikh, F.M., Callanan, A., Kavanagh, E.G., Burke, P.E., Grace, P.A., and McGloughlin, T.M. Fibrin: a natural biodegradable scaffold in vascular tissue engineering. Cells Tissues Organs **188,** 333, 2008.
2. Seliktar, D. Designing cell-compatible hydrogels for biomedical applications. Science **336,** 1124, 2012.
3. Dehghani, F., and Annabi, N. Engineering porous scaffolds using gas-based techniques. Curr Opin Biotechnol **22,** 661, 2011.
4. Fabiilli, M.L., Wilson, C.G., Padilla, F., Martín-Saavedra, F.M., Fowlkes, J.B., and Franceschi, R.T. Acoustic droplet-hydrogel composites for spatial and temporal control of growth factor delivery and scaffold stiffness. Acta Biomater **9,** 7399, 2013.
5. Zarem, H.A. Microcirculatory events within full-thickness skin allografts (homografts) in mice. Surgery **66,** 392, 1969.
6. Orr, A.W., Elzie, C.A., Kucik, D.F., and Murphy-Ullrich, J.E. Thrombospondin signaling through the calreticulin/LDL receptor-related protein co-complex stimulates random and directed cell migration. J Cell Sci **116,** 2917, 2003.
7. Demirdogen, B., Elcin, A.E., and Elcin, Y.M. Neovascularization by bFGF releasing hyaluronic acid-gelatin microspheres: in vitro and in vivo studies. Growth Factors **28,** 426, 2010.
8. Horio, T., Fujita, M., Tanaka, Y., *et al.* Efficacy of fragmin/protamine microparticles containing fibroblast growth factor-2 (F/P MPs/FGF-2) to induce collateral vessels in a rabbit model of hindlimb ischemia. J Vasc Surg **54,** 791, 2011.
9. Layman, H., Li, X.Y., Nagar, E., Vial, X., Pham, S.M., and Andreopoulos, F.M. Enhanced angiogenic efficacy through controlled and sustained delivery of FGF-2 and G-CSF from fibrin hydrogels containing ionic-albumin microspheres. J Biomat Sci Polym, E **23,** 185, 2012.
10. Dvir, T., Timko, B.P., Kohane, D.S., and Langer, R. Nanotechnological strategies for engineering complex tissues. Nat Nanotechnol **6,** 13, 2011.
11. Zhao, X., Kim, J., Cezar, C.A., *et al.* Active scaffolds for on-demand drug and cell delivery. Proc Natl Acad Sci U S A **108,** 67, 2011.
12. Stowers, R.S., Allen, S.C., and Suggs, L.J. Dynamic phototuning of 3D hydrogel stiffness. Proc Natl Acad Sci U S A **112,** 1953, 2015.
13. Adesanya, K., Vanderleyden, E., Embrechts, A., Glazer, P., Mendes, E., and Dubruel, P. Properties of electrically responsive hydrogels as a potential dynamic tool for biomedical applications. J Appl Polym Sci **131,** 41195, 2014.
14. Moncion, A., Arlotta, K.J., Kripfgans, O.D., *et al.* Design and characterization of fibrin-based acoustically responsive scaffolds for tissue engineering applications. Ultrasound Med Biol **42,** 257, 2016.
15. Moncion, A., Lin, M., O'Neill, E.G., *et al.* Controlled release of basic fibroblast growth factor for angiogenesis using acoustically-responsive scaffolds. Biomaterials **140,** 26, 2017.
16. Draijer, M., Hondebrink, E., van Leeuwen, T., and Steenbergen, W. Review of laser speckle contrast techniques for visualizing tissue perfusion. Lasers Med Sci **24,** 639, 2009.
17. Briers, J.D. Laser speckle contrast imaging for measuring blood flow. Opt Appl **37,** 139, 2007.
18. Dunn, A.K. Laser speckle contrast imaging of cerebral blood flow. Ann Biomed Eng **40,** 367, 2012.
19. Zhu, L., Niu, G., Fang, X., and Chen, X. Preclinical molecular imaging of tumor angiogenesis. Q J Nucl Med Mol Imaging **54,** 291, 2010.
20. Takahashi, H., Kato, K., Ueyama, K., *et al.* Visualizing dynamics of angiogenic sprouting from a three-dimensional microvasculature model using stage-top optical coherence tomography. Sci Rep **7,** 42426, 2017.
21. Cai, X., Zhang, Y.S., Xia, Y., and Wang, L.V. Photoacoustic microscopy in tissue engineering. Mater Today **16,** 67, 2013.
22. Ballyns, J.J., Gleghorn, J.P., Niebrzydowski, V., *et al.* Image-guided tissue engineering of anatomically shaped implants via MRI and micro-CT using injection molding. Tissue Eng Part A **14,** 1195, 2008.
23. Hendrikx, G., Vöö, S., Bauwens, M., Post, M.J., and Mottaghy, F.M. SPECT and PET imaging of angiogenesis and arteriogenesis in pre-clinical models of myocardial

ischemia and peripheral vascular disease. Eur J Nucl Med Mol Imaging **43,** 2433, 2016.
24. Ehling, J., Lammers, T., and Kiessling, F. Non-invasive imaging for studying anti-angiogenic therapy effects. Thromb Haemost **109,** 375, 2013.
25. Avigo, C., Flori, A., Armanetti, P., *et al.* Strategies for non-invasive imaging of polymeric biomaterial in vascular tissue engineering and regenerative medicine using ultrasound and photoacoustic techniques. Polym Int **65,** 734, 2016.
26. Browne, J.E., Watson, A.J., Hoskins, P.R., and Elliott, A.T. Validation of a sensitivity performance index test protocol and evaluation of colour Doppler sensitivity for a range of ultrasound scanners. Ultrasound Med Biol **30,** 1475, 2004.
27. Goertz, D.E., Yu, J.L., Kerbel, R.S., Burns, P.N., and Foster, F.S. High-frequency 3-D color-flow imaging of the microcirculation. Ultrasound Med Biol **29,** 39, 2003.
28. Xu, M., and Wang, L.V. Photoacoustic imaging in biomedicine. Rev Sci Instrum **77,** 041101, 2006.
29. Beard, P. Biomedical photoacoustic imaging. Interface focus **1,** 602, 2011.
30. Wang, L.V., and Hu, S. Photoacoustic tomography: in vivo imaging from organelles to organs. Science **335,** 1458, 2012.
31. Wang, X., Pang, Y., Ku, G., Xie, X., Stoica, G., and Wang, L.V. Noninvasive laser-induced photoacoustic tomography for structural and functional in vivo imaging of the brain. Nat Biotechnol **21,** 803, 2003.
32. Ogunlade, O., Ho, J.O., Kalber, T.L., *et al.* Monitoring neovascularization and integration of decellularized human scaffolds using photoacoustic imaging. Photoacoustics **13,** 76, 2019.
33. Talukdar, Y., Avti, P., Sun, J., and Sitharaman, B. Multimodal ultrasound-photoacoustic imaging of tissue engineering scaffolds and blood oxygen saturation in and around the scaffolds. Tissue Eng Part C Methods **20,** 440, 2014.
34. Zhu, Y., Xu, G., Yuan, J., *et al.* Light emitting diodes based photoacoustic imaging and potential clinical applications. Sci Rep **8,** 9885, 2018.
35. Hariri, A., Lemaster, J., Wang, J., Jeevarathinam, A.S., Chao, D.L., and Jokerst, J.V. The characterization of an economic and portable LED-based photoacoustic imaging system to facilitate molecular imaging. Photoacoustics **9,** 10, 2018.
36. Moncion, A., Arlotta, K.J., O'Neill, E.G., *et al.* In vitro and in vivo assessment of controlled release and degradation of acoustically responsive scaffolds. Acta Biomater **46,** 221, 2016.
37. Bashkatov, A.N., Genina, E.A., and Tuchin, V.V. Optical properties of skin, subcutaneous, and muscle tissues: a review. J Innov Opt Health Sci **4,** 9, 2011.
38. Martino, M.M., Briquez, P.S., Ranga, A., Lutolf, M.P., and Hubbell, J.A. Heparin-binding domain of fibrin (ogen) binds growth factors and promotes tissue repair when incorporated within a synthetic matrix. Proc Natl Acad Sci U S A **110,** 4563, 2013.
39. Jeon, O., Kang, S.-W., Lim, H.-W., Chung, J.H., and Kim, B.-S. Long-term and zero-order release of basic fibroblast growth factor from heparin-conjugated poly (L-lactide-co-glycolide) nanospheres and fibrin gel. Biomaterials **27,** 1598, 2006.
40. Jo, J., Lee, C.H., Kopelman, R., and Wang, X. In vivo quantitative imaging of tumor pH by nanosonophore assisted multispectral photoacoustic imaging. Nat Commun **8,** 471, 2017.
41. Yao, J., Maslov, K.I., Shi, Y., Taber, L.A., and Wang, LV. In vivo photoacoustic imaging of transverse blood flow by using Doppler broadening of bandwidth. Opt Lett **35,** 1419, 2010.

Address correspondence to:
Mario L. Fabiilli, PhD
Department of Biomedical Engineering
University of Michigan
1301 Catherine Street
Ann Arbor, MI 48109

E-mail: mfabiill@umich.edu

Xueding Wang, PhD
Department of Biomedical Engineering
University of Michigan
1301 Catherine Street
Ann Arbor, MI 48109

E-mail: xdwang@umich.edu

Received: June 5, 2019
Accepted: August 12, 2019
Online Publication Date: September 11, 2019